Tunable Bandgap GaInAsP Solar Cells With 18.7% Photoconversion Efficiency Synthesized by Low-Cost and High-Growth Rate Hydride Vapor Phase Epitaxy

Nikhil Jain, John Simon, Kevin L. Schulte, Daniel J. Friedman, David R. Diercks, Corinne E. Packard, David L. Young, and Aaron J. Ptak

***Abstract*—As market-dominant Si solar cell technology approaches its practical efficiency limit of 27.1%, a key challenge for the photovoltaic industry is to search for a low-cost ∼1.7 eV top cell that can enable cost-competitive tandems with solar-to-electricity conversion efficiency exceeding 30%. III-V semiconductors offer tunable bandgap and unparalleled efficiencies for tandem devices. However, their high manufacturing cost has been the biggest impediment for market entry. Hydride vapor phase epitaxy (HVPE) has recently reemerged as a promising low-cost alternative to incumbent metalorganic chemical vapor deposition (MOCVD) for III-V solar cells. Here, we show the first demonstration of ∼1.7 eV GaInAsP solar cells that achieve nearly 19% photoconversion efficiency synthesized by HVPE. The unprecedented growth rate of ∼42 μm/h achieved via HVPE (∼10× faster than conventional MOCVD) allowed the device layers to be deposited in less than seven minutes. Nearly abrupt and chemically distinct heterointerfaces were attained in spite of high-growth rates, which are known to exacerbate phase separation in GaInAsP alloys. Demonstration of ideality factor of $n = 1$ at max power point highlight the advancements in growth optimization and device design. The results presented here highlight a promising path toward tunable bandgap, high-growth rate, low-cost, and high-efficiency GaInAsP devices for direct solar-to-electricity and solar-to-hydrogen conversion.**

***Index Terms*—Dynamic-hydride vapor phase epitaxy (D-HVPE), GaInAsP, high-growth rate, phase separation, solar cell.**

Manuscript received February 15, 2018; revised June 19, 2018; accepted July 26, 2018. This work was authored by Alliance for Sustainable Energy, LLC, the manager and operator of the National Renewable Energy Laboratory for the U.S. Department of Energy (DOE) under Contract No. DE-AC36-08GO28308. "Funding provided by the U.S. Department of Energy Office of Energy Efficiency and Renewable Energy Solar Energy Technologies Office." *(Corresponding author: Nikhil Jain.)*

N. Jain, J. Simon, K. L. Schulte, D. J. Friedman, D. L. Young, and A. J. Ptak are with the National Renewable Energy Laboratory, Golden, CO 80401 USA (e-mail: jain34@vt.edu; john.simon@nrel.gov; kevin.schulte@nrel.gov; daniel.friedman@nrel.gov; David.Young@nrel.gov; aaron.ptak@nrel.gov).

D. R. Diercks is with the Department of Metallurgical and Materials Engineering, Colorado School of Mines, Golden, CO 80401 USA (e-mail: ddiercks@mines.edu).

C. E. Packard is with the National Renewable Energy Laboratory, Golden, CO 80401 USA, and also with the Department of Metallurgical and Materials Engineering, Colorado School of Mines, Golden, CO 80401 USA (e-mail: cpackard@mines.edu).

This paper has supplementary downloadable material available at http://ieeexplore.ieee.org.

Color versions of one or more of the figures in this paper are available online at http://ieeexplore.ieee.org.

Digital Object Identifier 10.1109/JPHOTOV.2018.2865172

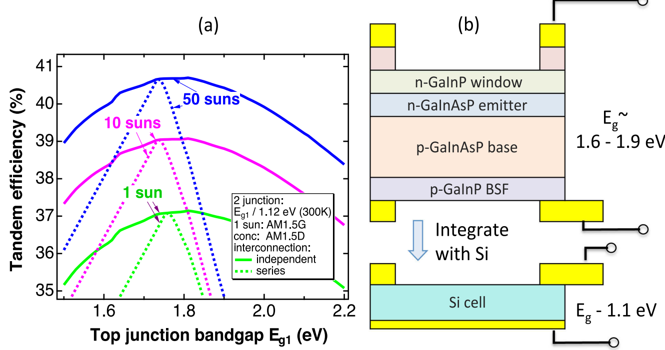

Fig. 1. (a) Projected one-sun and low-concentration dual-junction tandem solar cell efficiency versus top-cell bandgap (bottom-cell bandgap fixed to Si bandgap of 1.12 eV). (b) Envisioned integration scheme for realizing III-V/Si tandem architecture with GaInAsP top cell mechanically stacked onto a bottom Si solar cell (four-terminal). The top cell will be removed from the parent substrate to allow light to the bottom cell.

I. Introduction

Solar energy is the most abundant energy source and its annual potential far exceeds the world's total energy consumption [1]. According to the International Energy Agency's report, photovoltaics contributed to about 1.8% of the global electricity demand in 2016 [2]. For photovoltaics to contribute a substantial fraction of the world's electricity generation at terawatt scale, continued improvement in solar cell performance and at costs lower than traditional coal and natural gas is essential.

As the incumbent Si technology approaches its practical limit of 27.1% [3]–[5], Si-based tandems, in both series-connected (current-matched) and electrically independent configurations (such as four-terminals) have gained immense interest [6]–[12]. The tandems in four-terminal configuration are expected to outperform two-terminal tandems in terms of annual energy yields owing to the reduced spectral sensitivity [13]. These tandem cells could be particularly valuable for area-constrained and/or high-performance applications. It has been argued that a key challenge for the PV industry is the search for a low-cost top cell to realize Si-based tandems [7]. Fig. 1(a) shows the theoretical one-sun and low-concentration efficiencies for tandem solar cells with an Si bottom cell. As illustrated in the figure, top-cell materials in the bandgap range of 1.6–1.9 eV are ideal

2156-3381 © 2018 IEEE. Personal use is permitted, but republication/redistribution requires IEEE permission. See http://www.ieee.org/publications_standards/publications/rights/index.html for more information.

Pursuant to the DOE Public Access Plan, this document represents the authors' peer-reviewed, accepted manuscript. The published version of the article is available from the relevant publisher.

for Si-based tandems. Recently, perovskite/Si (1.63/1.1 eV) tandem reached 23.6% (two-terminal) efficiency, however this is still below single-junction Si efficiency primarily due to subpar top-cell performance of ∼14.5% [11]. In contrast, recently mechanically stacked dual-junction III-V/Si tandem solar cells with one-sun efficiencies up to 32.8% (four-terminal) have been demonstrated [9]. Despite their high-efficiencies, these III-V/Si tandems are not cost-competitive primarily due to the expensive GaAs substrate and III-V epitaxy [14], [15]. In order to mitigate the cost, substrate reuse technologies such as epitaxial lift-off and spalling have attracted considerable attention [14], [16]. However, III-V depositions are predominantly carried out by metalorganic chemical vapor deposition (MOCVD), which is costly owing to the expensive metalorganic precursors, relatively lower throughput, and typical growth rates of 1 to 6 μm/h. There is a strong desire to develop a tunable bandgap, high-growth rate, low-cost, and high-efficiency ∼1.7 eV junction, which could have a transformative impact on solar-to-electricity and solar-to-hydrogen conversion efficiencies [7], [17]. Quaternary GaInAsP compound semiconductor alloys are promising aluminum-free candidates for ∼1.7 eV junction, however are challenging alloys to synthesize due to their propensity for phase separation [19], [20].

In this paper, we demonstrate GaInAsP cells that incorporate GaInP window layers for front surface passivation grown on a custom-built dual-chamber HVPE reactor [18] (hereafter referred as dynamic-HVPE or D-HVPE). We characterize complex interfaces between ternary and quaternary alloys using transmission electron microscopy and demonstrate chemically distinct heterointerfaces. The GaInAsP absorber layer is grown at ∼0.7 μm/min—about 10x faster than typical MOCVD reports on similar alloys [19], [20]. We present GaInAsP solar cells that achieve a one-sun photoconversion efficiency of nearly 19%, highlighting the viability of D-HVPE to grow nearly abrupt heterointerfaces. Key factors limiting the performance are identified using device modeling and directions for future improvements are discussed.

A. Low-Cost and High-Efficiency III-V/Si Tandems—The Case for HVPE and GaInAsP as the Top-Cell Candidate

It is imperative to develop alternative low-cost III-V deposition techniques that could allow III-V/Si tandems to become cost-competitive. HVPE has recently reemerged as a promising low-cost alternative for III-V solar cell growth as it can attain significantly higher growth rates than MOCVD (up to 300 μm/h) [21] and uses much lower Group V overpressures. Additionally, the elemental Group-III metal sources offer an unprecedented cost advantage compared with the expensive metalorganic precursors used in MOCVD (∼10x cost savings) [22]. Our custom-built, dual-chamber D-HVPE reactor can enable high-quality epitaxial heterointerfaces, which have traditionally been challenging to grow in single-chamber reactors [23]–[25]. Single-junction GaAs [26] and GaInP [27] solar cells grown by D-HVPE have been recently demonstrated, but they do not offer the bandgap tunability desired for Si-tandems. Quaternary GaInAsP alloys present a promising aluminum-free top-cell candidate with bandgap tunability in the range of ∼1.6–1.9 eV and can also be grown lattice-matched to GaAs (see Supplementary Fig. 1). $Al_xGa_{1-x}As$ alloys also offer similar bandgap tunability but have been reported to form deep-level recombination defects due to oxygen contamination [28] that may hinder long-term performance and reliability. A proposed integration scheme for realizing a Si-tandem stack (e.g., GaInAsP/Si) is illustrated in Fig. 1(b). Another integration approach could leverage surface mediated wafer bonding as discussed in [10]. Besides the potential for solar cells, tandem architectures with a top-junction bandgap close to ∼1.7 eV are also ideal for solar-to-hydrogen production via photoelectrochemical water splitting [17] and are desirable for noninvasive biomedical applications using ∼730 nm laser diodes [29].

II. Experimental Methods

The tandem solar cell performance modeling [see Fig. 1(a)] was performed for both series-connected and independently connected configurations of idealized cells. The open-circuit voltage (V_{OC}) of the top cells was determined using the detailed balance calculations, while the dark current of the silicon cell was assumed to have ideality $n = 1$ with reverse saturation current $J_{01} = 1.28 \times 10^{-11}$mA/ cm^2, such that its V_{OC} = 0.72 V when short-circuit current density, J_{SC} = 16 mA/ cm^2. This approximates the dark current of the best experimentally demonstrated silicon cells [5]. A filter layer representing AlInP window was included to simulate absorption in the window layer. The J_{SC} of the top junction was calculated using shifted GaAs absorption coefficients (in energy) and assuming that every photon absorbed is converted into current. The top junction was thinned for maximizing the efficiency at each point for series-connected configuration. The J_{SC} of the bottom silicon junction was calculated from the spectrum filtered by the thinned top junction, assuming that every photon absorbed by the bottom junction is collected as current. Losses such as grid shadowing, series resistance, and reflectance are assumed to have negligible contribution in this model.

The GaInAsP solar cell structures were grown in a custom-built atmospheric pressure, dual-chamber D-HVPE reactor [18]. Metal chlorides (GaCl, InCl), which are formed upstream by the reaction of HCl gas with elemental Ga or In at 800 °C, were used as Group-III sources. Arsine (AsH_3) and phosphine (PH_3) gases were used as Group-V precursors. Hydrogen selenide and diethylzinc were used as the n- and p-type dopant precursors, respectively. The growth zone temperature was maintained at 625 °C in both growth chambers. Depositing these epitaxial layers at relatively low growth temperature (625 °C) is expected to suppress phase separation by kinetically limiting the growth to facilitate metastable growth of GaInAsP alloy [20], [30]–[32]. All epitaxial layers were grown on (001) GaAs:Zn substrates with a 4° miscut toward (111)B (see Supplementary material for growth details).

Preliminary solar cell designs were focused on unpassivated front heterojunction (FHJ) GaInAsP devices with a GaInP emitter layer. These early stage diagnostic devices did not have a high bandgap window layer for front passivation [shown in Fig. 2(b)].

Pursuant to the DOE Public Access Plan, this document represents the authors' peer-reviewed, accepted manuscript. The published version of the article is available from the relevant publisher.

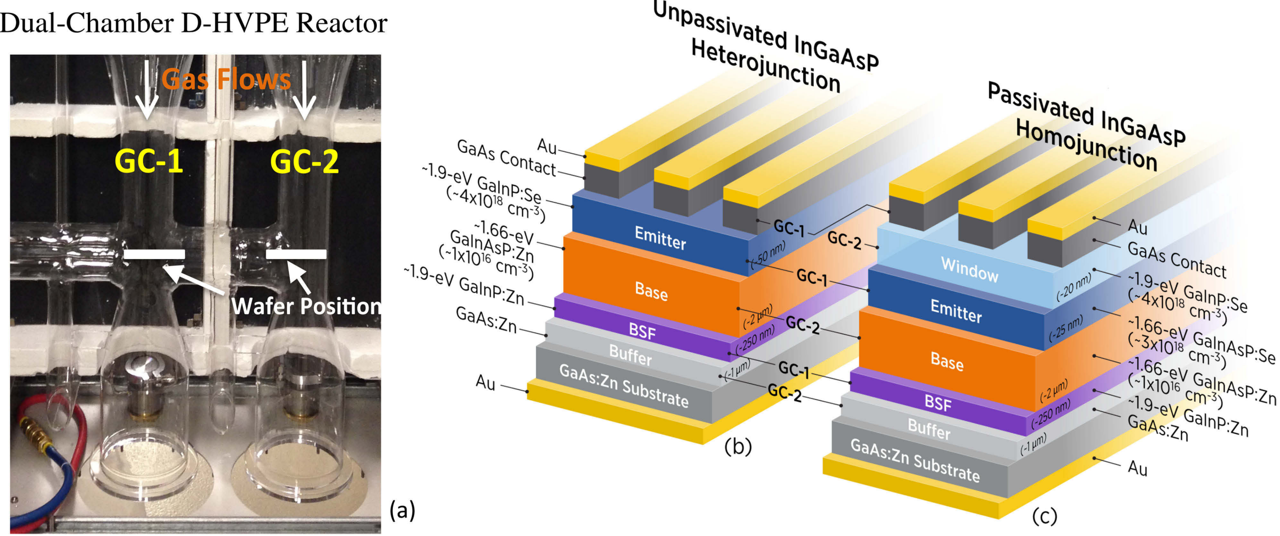

Fig. 2. (a) Dual-chamber D-HVPE reactor separated via hydrogen curtain; GC-1 and GC-2 are the two interconnected growth chambers. (b) Device schematic of unpassivated GaInAsP heterojunction cell. (c) Schematic of passivated GaInAsP homojunction solar cell with GaInP window layer.

The solar cell structures were grown upright and the $\sim$2 μm thick GaInAsP:Zn base layer of all the devices was grown at $\sim$0.7 μm/min or $\sim$42 μm/h. Homojunction GaInAsP solar cells (with GaInAsP emitter and base) with front surface passivating window layer were developed [shown in Fig. 2(c)] in an attempt to enhance the short-wavelength carrier collection and the overall cell efficiency. The structural quality of quaternary GaInAsP epilayers and the solar cell heterointerfaces were characterized using transmission electron microscopy. Cross-sectional lift-out specimens oriented along a 110 were removed from the device structure using a Helios NanoLab 600i SEM/FIB DualBeam workstation. Microscopy and energy dispersive X-ray spectroscopy (EDS) were performed on these specimens with an FEI Talos F200X field emission scanning/transmission electron microscope at 200 keV.

All the solar cells were processed with electroplated Ni/Au as the front contact and electroplated Au as the back Ohmic contact layer. Cells were 0.5 $\times$ 0.5 cm or 0.25 cm^2 in area. A bilayer MgF_2/ZnS (92 nm/51 nm) antireflection coating was deposited using thermal evaporation (see Supplementary Table II for complete processing details). Capacitance–voltage (*CV*) and room-temperature Hall effect measurements were performed to determine the n-type and p-type dopant concentrations in the base and the emitter layers, respectively. The quantum efficiency (QE) and specular reflectance were measured on a custom-built QE set-up, and current density–voltage (*J*–*V*) measurements were performed on an XT10 solar simulator, tuned to simulate AM1.5G spectrum at 1000 W/m^2, with a primary calibration reference cell used to set intensity.

III. Results and Discussion

The growth of GaInAsP alloys has historically been challenging owing to a wide miscibility gap, which makes these alloys susceptible to phase separation [30]–[32]. Studies on HVPE-grown GaInAsP alloys have been previously reported [23]–[25], [33]. However, GaInAsP solar cells grown by HVPE have not been given attention. We have developed a recipe (see Supplementary Table I) to grow lattice-matched GaInAsP epitaxial films on a GaAs substrate by D-HVPE [reactor shown in Fig. 2(a)]. The nominal growth rate of GaInAsP films ($E_g \sim$ 1.66 eV) was determined to be $\sim$0.7 μm/min or $\sim$42 μm/h using layer thickness determined from SEM and known growth time. Even though there is potential to further increase the growth rate, no such attempts were made in this study. We estimate the composition of the GaInAsP film to be Ga $\sim$ 72%, In $\sim$28%, As-34%, and P-56%, assuming a GaAs lattice-constant of 5.653 Å and a bandgap of $\sim$1.66 eV (assuming no atomic ordering). Precise composition estimation will require chemical analysis using techniques such as Rutherford backscattering spectrometry. The high-growth rate GaInAsP epitaxial films showed smooth surface morphology with a root-mean square roughness of $\sim$0.45 nm over a scan area of 25 $\times$ 25 μm (see Supplementary Fig. 3). We investigated the photoluminescence response (see Supplementary Fig. 2) and also assessed the optical thickness of GaInAsP alloys prior to building a full solar cell device stack. Using experimentally determined optical constants, we evaluated that nearly 95% of the incident photons can be absorbed in a 2 μm thick GaInAsP absorber l (see Supplementary Fig. 4). Note that the bandgap of GaInAsP alloy is lower than optimal bandgap as modeled in Fig. 1(a). This was primarily due to the inability to flow lower amount of AsH_3 gas (mass flow controller limitation) in our current reactor configuration (see Supplementary Table I) to maintain lattice matching. We should be able to overcome this with modest hardware changes in the future.

A. *Unpassivated Front Heterojunction GaInAsP Solar Cells*

The dual-chamber reactor design allows independent control of the gas flows, which is necessary to grow subsequent III-V layers without growth interruptions or pauses during the growth

Pursuant to the DOE Public Access Plan, this document represents the authors' peer-reviewed, accepted manuscript. The published version of the article is available from the relevant publisher.

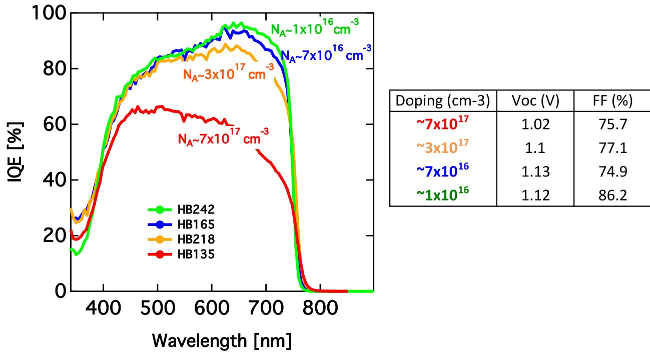

Doping (cm-3)	Voc (V)	FF (%)
~7x10^17	1.02	75.7
~3x10^17	1.1	77.1
~7x10^16	1.13	74.9
~1x10^16	1.12	86.2

Fig. 3. Internal quantum efficiency of GaInAsP solar cells with varying p-type base doping. The V_{OC} and FF for the respective devices are shown in the corresponding table. These devices did not have any antireflection coating.

[18], [34] (see Supplementary material for details on reactor configuration, growth sequence and growth recipe). Preliminary solar cell designs were focused on FHJ GaInAsP devices with a p-type GaInAsP:Zn base (absorber) layer ($E_g \sim 1.66$ eV) and an n-type GaInP:Se heterojunction emitter ($E_g \sim 1.90$ eV). The bandgap of the solar cell was determined by the detailed-balance equivalence method as described in [35]. Front hetereojunction design was the preliminary cell design choice since the structure is essentially a double heterostructure and enables faster feedback on the development of GaInAsP absorber growth conditions. The nominal thicknesses and doping concentrations of the respective layers are included in the solar cell device schematic as shown in Fig. 2(b).

The unpassivated heterojunction GaInAsP cell design lacked a higher bandgap window layer for front surface passivation of the emitter layer (hereafter, this structure is referred to as an unpassivated heterojunction). Hence, a high-level of front surface recombination is expected. The high bandgap GaInP emitter should suppress dark current and potentially improve the V_{OC}. The base doping concentration was optimized to maximize the conversion efficiency. The long-wavelength photoresponse (primarily representative of collection in the thick base layer) was found to be very sensitive to base doping (see Fig. 3). The V_{OC} and fill factor (FF) for the respective devices are shown in the corresponding table. Note that the reason for this improvement is not clear at present. Lowering the base doping led to significantly improved device performance (collection length, FF and ideality $n = 1$) likely due to the suppression of recombination (see DIV in Supplementary Fig. 5) associated with phase separation in the metastable GaInAsP absorber. Reduction in J_{02} contributed to improvement in V_{oc} and FF as well. Similar phenomenon of improvement in collection length with reduction of Zn doping in GaInAsP absorber material has been reported for MOCVD grown material as well [20], [36]–[38].

The EQE and J–V curves of the solar cells corresponding to the unpassivated heterojunctions are shown in Fig. 4(a) and (b), respectively (in purple). These devices with peak EQEs exceeding 90% near the GaInAsP band-edge highlight promising collection properties of the optimized GaInAsP absorber material. It is worth noting that these unpassivated heterojunction GaInAsP solar cells showed a rather poor short-wavelength photoresponse (below 650 nm) due to the lack of front passivation. Evidently, the unpassivated and heavily doped GaInP emitter layer limited the short-circuit current density (J_{SC}) to 16.4 mA/ cm^2. The V_{OC} of 1.15 V and a FF of 82.6% translated to a solar-to-electricity conversion efficiency of 15.6% under one-sun illumination. However, this efficiency is not sufficient for Si-tandems to exceed the efficiency of single-junction Si cells, thus necessitating the improvement of the device structure to push the efficiency closer to 20% for the top 1.7 eV junctions.

B. Passivated GaInAsP Homojunction Solar Cells With Window

Development of lattice-matched cladding layers is critical to achieve the surface passivation necessary to enable high-efficiency devices. The cladding layers must be designed using higher bandgap alloys to minimize parasitic absorption and must provide a sufficient energy barrier to reflect the minority carriers. Homojunction GaInAsP ($E_g \sim 1.66$ eV) solar cells were developed with both the n- and p-side of the junction made from GaInAsP alloys of nominally the same composition, as shown in the device schematic in Fig. 2(c). Both sides of the junction were cladded with a GaInP ($E_g \sim 1.90$ eV) layer as the passivating layer. Note that a higher bandgap AlInP window layer would be the preferred choice to minimize front absorption losses. However, AlCl formed in HVPE is known to attack the fused SiO_2 reactor wall, thus damaging the apparatus and resulting in high background Si doping [39]. An additional challenge is preventing the oxidation of metallic Al source [39]. Therefore, our generation-1 reactor does not have Al source. Note that this is not a fundamental HVPE growth technique limitation. For our design, the adoption of GaInP front window as the front passivation layer is still expected to substantially improve the short-wavelength carrier collection for ~1.7 eV GaInAsP solar cells. The EQE and J–V curves representative of the passivated homojunction GaInAsP solar cells with a GaInP window layer are shown in Fig. 4(a) and (b), respectively (in green). The device data for the unpassivated GaInAsP cell with similar base doping ($N_A \sim 1 \times 10^{16}$ cm^{-3}) is also plotted for direct comparison (in purple). The passivated homojunction cell showed a substantial improvement in the short-wavelength photoresponse, translating to an ~18% boost in the J_{SC} (16.4–19.2 mA/cm^2), indicating the effectiveness of front surface passivation. The improvement in short-wavelength photoresponse translated to an absolute ~3% gain in the one-sun cell efficiency. The J-V curve of the champion GaInAsP solar cell (independently certified by NREL) is shown in the Supplementary Fig. 9. The best cell demonstrated a V_{OC} of 1.13 V, J_{SC} of 19.2 mA/cm^2, and an FF of 85.4%, translating to a conversion efficiency of 18.7%. It is worth mentioning that the total deposition time for the full homojunction solar cell grown by D-HVPE was less than seven minutes (not including the substrate heat-up and cool down).

Table I gives an overview of the solar cell parameters for the two device structures discussed. The apparent ~20 mV drop in V_{OC} for the homojunction cell in comparison with the heterojunction cells is primarily attributed to the lower bandgap (GaInAsP) emitter layer in homojunction cells.

Pursuant to the DOE Public Access Plan, this document represents the authors' peer-reviewed, accepted manuscript. The published version of the article is available from the relevant publisher.

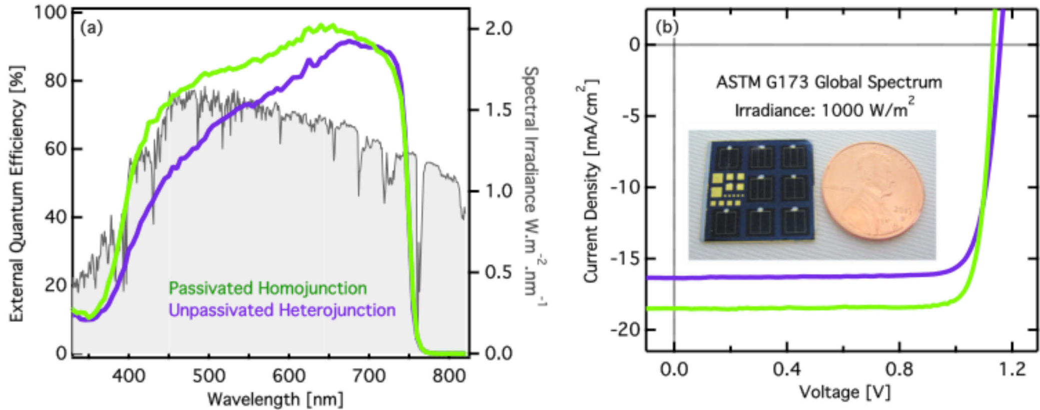

Fig. 4. (a) EQE and (b) light J–V curves (under AM1.5G) for passivated (green) and unpassivated (purple) GaInAsP solar cells grown at ~0.7 μm/min. These devices include a front-side bilayer MgF_2/ZnS antireflection coating. The base thickness is ~2 μm and the base doping, N_A, is $\sim 1 \times 10^{16}$ cm^{-3}. Inset in Fig. 4(b) shows a representative sample (AR coated) with eight individual 0.25 × 0.25 cm^2 GaInAsP homojunction solar cells.

TABLE I
GAINASP SOLAR CELL PERFORMANCE PARAMETERS (WITH ARC) MEASURED UNDER THE AM1.5G SPECTRUM-1000 W/M^2

Sample (Base Thickness)	V_{OC} (V)	W_{OC} (V)	J_{SC} (mA/cm^2)	FF (%)	Efficiency (%)
Unpassivated Heterojunction	1.15	~0.51	16.4	82.6	15.6
Passivated Homojunction	1.13	~0.53	19.2	85.4	18.7

A bandgap-voltage offset, $W_{OC} = E_g/q - V_{OC}$ of ~0.53 V suggests that there is room for further improvement in the homojunction device performance. In comparison with the best MOCVD-grown GaInAsP solar cells reported in the literature [20], the D-HVPE grown cells in this paper are about 2%–3% less efficient. The slightly higher V_{OC} in MOCVD grown solar cells (1.18 V by MOCVD compared with 1.13 V by D-HVPE) could be attributed to the higher bandgap GaInP emitter and the presence of gold back reflector aiding photon recycling (see Supplementary material for comparison with MOCVD devices). It is also worth noting that these solar cells synthesized at high-growth rate achieved a narrow statistical distribution (see Supplementary Fig. 6), attesting to the ability of the D-HVPE technique to produce fairly uniform devices comprising of complex quaternary and ternary alloys.

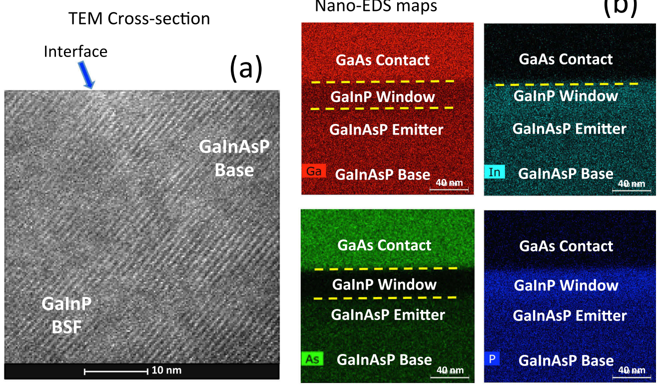

Fig. 5. High-resolution <110> bright field TEM cross-sectional image of GaInP BSF and GaInAsP base heterointerfaces for the GaInAsP homojunction device. (b) EDS elemental map showing minimal chemical intermixing between the device layers.

C. *Heterointerface Characterization Using Transmission Electron Microscopy*

The heterointerfaces of the GaInAsP homojunction solar cell were characterized using transmission electron microscopy. A cross-sectional lift-out specimen of the device displayed in Fig. 2(c) was prepared as outlined in the experimental section. Fig. 5(a) presents a high-resolution 110 bright field image showing a nearly flat heterointerface between the GaInP back surface field (BSF) and the GaInAsP base layer, which is highlighted by the blue arrow. Individual elemental maps were also acquired using EDS. The elemental maps representing the various heterointerfaces of the solar cell structure are shown in Fig. 5(b). These maps reveal negligible chemical intermixing between the respective device layers, highlighting the viability of the D-HVPE technique to grow complex III-V devices (quaternary and ternary layers) with nearly abrupt heterointerfaces, even for the growth of thin epitaxial layers at very high rates. Note that complementary structural analyses are necessary to evaluate the extent of the remaining phase separation.

D. *Device Modeling and Analysis*

It has been argued that phase separation could affect minority carrier properties such as diffusion length [20], [40]. In order to gain insight into the underlying physics of carrier transport and understand the performance-limiting factors, we modeled the EQE and J–V characteristics of the passivated homojunction

Pursuant to the DOE Public Access Plan, this document represents the authors' peer-reviewed, accepted manuscript. The published version of the article is available from the relevant publisher.

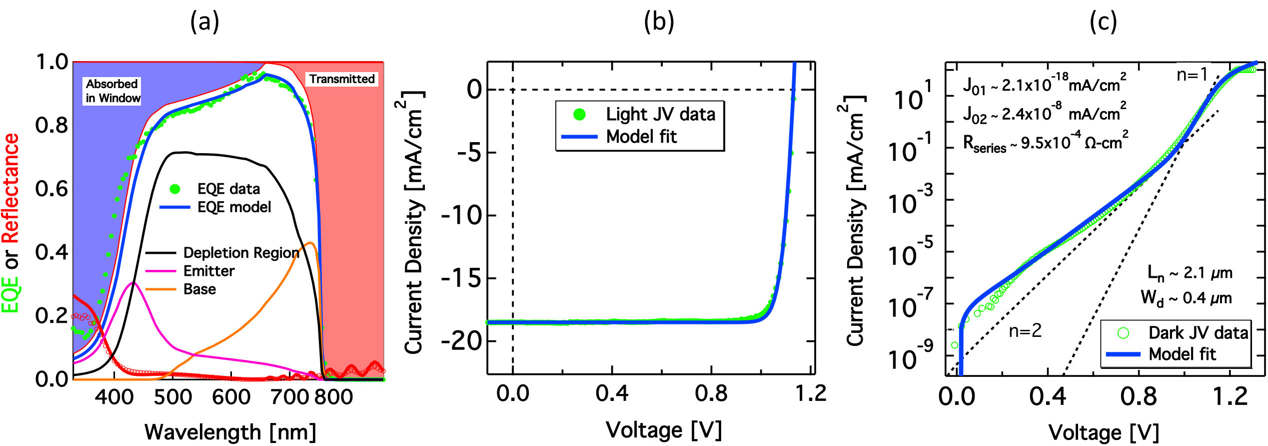

Fig. 6. Modeled (blue line) and experimental data (green dots) for 18.7% passivated GaInAsP homojunction solar cell representing (a) EQE. (b) Light *J–V*. (c) Dark *J–V* fits. Modeling was performed using Hovel's drift-diffusion equations [41] to extract minority carrier transport properties. The data in this figure are for the same passivated homojunction device data as shown in Fig. 4.

GaInAsP solar cells using Hovel's drift-diffusion equations [41]. Simultaneous fits to the EQE and *J–V* curves for a two-diode model incorporating series and shunt resistance are plotted in Fig. 6. The slight discrepancy in the short-wavelength fit of the EQE could be attributed to subtle differences in the thickness or composition of the GaInP window layer. Model fit to the experimental EQE data [see Fig. 6(a)] allowed us to evaluate the collection contribution from various device layers, namely, the emitter (in pink), the base (in orange), and the depletion region (in black). The depletion approximation allowed us to estimate a depletion width of $\sim$0.4 μm at a p-type doping concentration of 1×10^{16} cm^{-3}, which was further confirmed from electrical *C-V* measurements. The modeling also allowed us to estimate a minority carrier diffusion length (L_n) of $\sim$2.1 μm for the GaInAsP:Zn base layer. Therefore, it is apparent that the overall collection length exceeds the 2 μm thick GaInAsP base layer, which is nearly the optimal desired thickness for GaInAsP absorbers as discussed previously (see Supplementary Fig. 4). It is also worth noting that the dark *J–V* plots [see Fig. 6(c)] indicate that the diode behavior transitions from an ideality factor of $n = 2$ (depletion-region nonradiative recombination-limited) to an ideality factor of $n = 1$ (diffusion-region radiative recombination-limited) at the maximum power point which is the signature characteristic of an ideal diode. Thus, despite the propensity for phase separation, collection length exceeding the optical thickness and the demonstration of ideal diode characteristic represent promising material quality for GaInAsP absorber grown at very high rates by D-HVPE.

E. *Pathways for Future Improvement and Outlook*

Future efforts to improve the device performance should predominantly be directed toward improving the V_{OC}. Since the diode behavior at the maximum power point is representative of $n = 1$ ideal diode, reducing the recombination in the quasi-neutral region and at the interfaces should boost the V_{OC}. Exploring growth conditions (temperature, V/III ratio) that could influence the bulk GaInAsP material quality could be a promising avenue. Additionally, the development of a higher bandgap GaInAsP emitter could reduce the dark current associated with diffusion-region limited recombination (J_{01}) and potentially drive gains in both V_{OC} and FF. Incorporation of an even wider bandgap window layer (such as AlInP, $E_g \sim 2.25$ eV) is expected to improve the short-wavelength carrier collection. These cumulative developments are expected to advance the performance of GaInAsP solar cells to well over 20% in efficiency.

IV. Conclusion

Development of new energy materials and deposition techniques could enable next generation of devices which could outcompete the incumbent technology and open innovative avenues for not only terrestrial energy but for novel portable power applications as well. High-efficiency and low-cost $\sim$1.7 eV solar cells are highly sought for the development of tandem architectures necessary to push the efficiency limits for solar-to-electricity (beyond 30%) and solar-to-hydrogen conversion (beyond 20%).

We demonstrate $\sim$1.7 eV GaInAsP solar cells yielding nearly 19% photoconversion efficiency synthesized by D-HVPE. Understanding the synergistic design tradeoffs between the optical absorption and carrier collection enabled solar cells with peak QE exceeding 95%. The unprecedented growth rate of $\sim$0.7 μm/min or $\sim$42 μm/h attained via D-HVPE ($\sim$10x faster than conventional MOCVD) allowed the device layers to be deposited in less than seven minutes. Despite the propensity for phase separation in GaInAsP alloys, which is exacerbated at higher growth rates, device modeling suggests that the diffusion length exceeds or at least equals the optimal optical thickness of 2 μm and the diode behaves like an ideal diode at the maximum power point. Furthermore, the nearly abrupt and chemically distinct heterointerfaces, achieved in spite of the high-growth rates, highlight the viability of the D-HVPE to grow III-V devices with complex designs. The results presented here showcase a promising path toward tunable bandgap, high-growth rate, low-cost, and high-efficiency GaInAsP devices, which are highly sought-after for applications spanning noninvasive biomedical surgery, solar-to-electricity, and solar-to-hydrogen production.

Pursuant to the DOE Public Access Plan, this document represents the authors' peer-reviewed, accepted manuscript. The published version of the article is available from the relevant publisher.

ACKNOWLEDGMENT

The authors would like to acknowledge M. Young and D. Guiling for assistance in cell processing and epitaxial growth. The authors would also like to acknowledge the technical discussions with the III-V team at NREL. A. Hicks at NREL assisted with graphical device schematics. ~~"This work was authored by Alliance for Sustainable Energy, LLC, the manager and operator of the National Renewable Energy Laboratory for the U.S. Department of Energy (DOE) under Contract No. DE-AC36-08GO28308.~~ The views expressed in the article do not necessarily represent the views of the DOE or the ~~United States~~ Government. The ~~United States~~ Government retains and the publisher, by accepting the article for publication, acknowledges that the ~~United States~~ Government retains a nonexclusive, paid-up, irrevocable, worldwide license to publish or reproduce the published form of this work, or allow others to do so, for ~~United States~~ Government purposes."

REFERENCES

[1] N. M. Haegel *et al.*, "Terawatt-scale photovoltaics: Trajectories and challenges," *Science*, vol. 356, pp. 141–143, 2017.

[2] International Energy Agency 2016 Snapshot of Global Photovoltaic Markets (International Energy Agency Photovoltaic Power System Programme), 2017. [Online]. Available: http://www.ieapvps.org/fileadmin/dam/public/report/statistics/IEA-PVPS_-__A_Snapshot_of_Global_PV_-_1992-2016.pdf

[3] A. Richter, M. Hermle, and S. W. Glunz, "Reassessment of the limiting efficiency for crystalline silicon solar cells," *IEEE J. Photovolt.*, vol. 3, no. 4, pp. 1184–1191, Oct. 2013.

[4] K. Yoshikawa *et al.*, "Silicon heterojunction solar cell with interdigitated back contacts for a photoconversion efficiency over 26%," *Nature Energy*, vol. 2, 2017, Art. no. 17032.

[5] M. A. Green *et al.*, "Solar cell efficiency tables (version 49)," *Prog. Photovolt., Res. Appl.*, vol. 25, pp. 3–13, 2017.

[6] M. A. Green and S. P. Bremner, "Energy conversion approaches and materials for high-efficiency photovoltaics," *Nature Mater.*, vol. 16, pp. 23–34, 2017.

[7] M. A. Green, "Commercial progress and challenges for photovoltaics," *Nature Energy*, vol. 1, 2016, Art. no. 15015.

[8] N. Jain and M. K. Hudait, "III-V multijunction solar cell integration with silicon: present status, challenges and future outlook," *Energy Harvesting Syst.*, vol. 1, nos. 3/4, pp. 121–145, 2014.

[9] S. Essig *et al.*, "Dual-junction III-V/Si solar cells with over 30% one-sun efficiency," *Nature Energy*, vol. 2, no. 9, 2017, Art. no. 17144.

[10] R. Cariou *et al.*, "Monolithic two-terminal III-V//Si triple-junction solar cells with 30.2% efficiency under 1-Sun AM1.5g," *IEEE J. Photovolt.*, vol. 7, no. 1, pp. 367–373, Jan. 2017.

[11] K. A. Bush *et al.*, "23.6%-efficient monolithic perovskite/silicon tandem solar cells with improved stability," *Nature Energy*, vol. 2, 2017, Art. no. 17009.

[12] Z. Yu, M. Leilaeioun, and Z. Holman, "Selecting tandem partners for silicon solar cells," *Nature Energy*, vol. 1, 2016, Art. no. 16137.

[13] H. Liu *et al.*, "The realistic energy yield potential of GaAs-on-Si tandem solar cells: a theoretical case study," *Opt. Express*, vol. 23, no. 7, pp. A382–A390, 2015.

[14] J. S. Ward *et al.*, "Techno-economic analysis of three different substrate removal and reuse strategies for III-V solar cells," *Prog. Photovolt., Res. Appl.*, vol. 24, pp. 1284–1292, 2016.

[15] M. Woodhouse and A. Goodrich, "A manufacturing cost analysis relevant to single- and dual-junction photovoltaic cells fabricated with III-Vs and III-Vs grown on Czochralski silicon," NREL, Golden, CO, USA, NREL/PR-6A20-60126, 2013.

[16] C. A. Sweet *et al.*, "Controlled exfoliation of (100) GaAs-based devices by spalling fracture," *Appl. Phys. Lett.*, vol. 108, 2016, Art. no. 011906.

[17] J. L. Young *et al.*, "Direct solar-to-hydrogen conversion via inverted metamorphic multi-junction semiconductor architectures," *Nature Energy*, vol. 2, 2017, Art. no. 17028.

[18] D. L. Young, A. J. Ptak, T. F. Kuech, K. L. Schulte, and J. Simon, "High throughput semiconductor deposition system," U.S. Patent 20 130 309 848, 2013.

[19] P. R. Sharps *et al.*, "Development of 20% efficient GaInAsP solar cells," in *Proc. 23rd IEEE Photovolt. Spec. Conf.*, 1993, pp. 633–638.

[20] N. Jain, J. F. Geisz, R. M. France, A. G. Norman, and M. A. Steiner, "Enhanced current collection in 1.7 eV GaInAsP solar cells grown on GaAs by metalorganic vapor phase epitaxy," *IEEE J. Photovolt.*, vol. 7, no. 3, pp. 927–933, May 2017.

[21] M. Deschler *et al.*, "Very rapid growth of high quality GaAs, InP and related III-V compounds," *J. de Physique*, vol. 49, pp. 689–692, 1988.

[22] M. Woodhouse *et al.*, "Supply-Chain dynamics of tellurium, indium, and gallium within the context of PV module manufacturing costs," *IEEE J. Photovolt.*, vol. 3, no. 2, pp. 833–837, Apr. 2013.

[23] T. Mizutani *et al.*, "Vapor phase growth of GaInAsP/InP DH structures by the dual-growth-chamber method," *Jpn. J. Appl. Phys.*, vol. 19, pp. L113–L116, 1980.

[24] T. Nishibe and M. Iwamoto, "Hydride VPE growth technique for InP/GaInAsP system," *J. Cryst. Growth*, vol. 94, pp. 588–596, 1989.

[25] K. Sugiyama, H. Kojima, H. Enda, and M. Shibata, "Vapor phase epitaxial growth and characterization of $Ga_{1-y}In_yAs_{1-x}P_x$ quaternary alloys," *Jpn. J. Appl. Phys.*, vol. 16, no. 12, pp. 2197–2203, 1977.

[26] J. Simon *et al.*, "Upright and inverted single junction GaAs solar cells grown by hydride vapor phase epitaxy," *IEEE J. Photovolt.*, vol. 7, no. 1, pp. 157–161, Jan. 2017.

[27] K. L. Schulte *et al.*, "Development of GaInP solar cells grown by hydride vapor phase epitaxy," *IEEE J. Photovolt.*, vol. 7, no. 4, pp. 1153–1158, Jul. 2017.

[28] S. Heckelmann, D. Lackner, C. Karcher, F. Dimroth, and A. W. Bett, "Investigations on AlGaAs solar cells grown by MOVPE," *IEEE J. Photovolt.*, vol. 5, no. 1, pp. 446–453, Jan. 2015.

[29] E. Nomoto *et al.*, "700-730 nm GaInAsP quantum well ridge-waveguide lasers," *Proc. SPIE*, vol. 6909, 2008, Art. no. 69091C.

[30] K. Onabe, "Calculation of miscibility gap in quaternary InGaPAs with strictly regular solution approximation," *Jpn. J. Appl. Phys.*, vol. 21, pp. 797–798, 1982.

[31] Y. Konaka, K.-I. Ono, Y. Terai, and Y. Fujiwara, "Coexistence properties of phase separation and CuPt-ordering in GaInAsP grown on GaAs substrates by organometallic vapor phase epitaxy," *J. Cryst. Growth*, vol. 312, pp. 2056–2059, 2010.

[32] K. Ono, M. Takemi, and Y. Fujiwara, "Metalorganic vapor phase epitaxial growth parameter dependence of phase separation in miscibility gap of InGaAsP," *Jpn. J. Appl. Phys.*, vol. 47, no. 2, pp. 896–898, 2008.

[33] N. Jain *et al.*, "InGaAsP solar cells grown by hydride vapor phase epitaxy," in *Proc. 43rd IEEE Photovolt. Spec. Conf.*, Portland, OR, USA, 2016, pp. 1–5.

[34] K. L. Schulte, J. Simon, D. L. Young, and A. J. Ptak, "Computational fluid dynamics-aided analysis of a hydride vapor phase epitaxy reactor," *J. Cryst. Growth*, vol. 434, pp. 138–147, 2016.

[35] J. F. Geisz *et al.*, "Generalized optoelectronic model of series-connected multijunction solar cells," *IEEE J. Photovolt.*, vol. 5, no. 6, pp. 1827–1839, Nov. 2015.

[36] G. J. van Gurp, T. van Dongen, G. M. Fontijn, J. M. Jacobs, and D. L. A. Tjaden, "Interstitial and substitutional Zn in InP and InGaAsP," *J. Appl. Phys.*, vol. 65, pp. 553–560, 1989.

[37] W. E. Plano, D. W. Nam, J. S. Major, K. C. Hsieh, and N. Holonyak, "Column III and V ordering in InGaAsP and GaAsP grown on GaAs by metalorganic chemical vapor deposition," *Appl. Phys. Lett.*, vol. 53, pp. 2537–2539, 1988.

[38] H. H. Park, K. H. Lee, and D. A. Stevenson, "Zn diffusion enhancement of interdiffusion in a GaAs-InGaPAs heterostructure," *Appl. Phys. Lett.*, vol. 53, pp. 2299–2301, 1988.

[39] M. Ettenberg, A. G. Sigai, A. Dreeben, and S. L. Gilbert, "Vapor growth and properties of AlAs," *J. Electrochem. Soc.*, vol. 118, no. 8, pp. 1355–1358, 1971.

[40] R. R. LaPierre, T. Okada, B. J. Robinson, D. A. Thompson, and G. C. Weatherly, "Spinodal-like decomposition of grown by gas source molecular beam epitaxy," *J. Cryst. Growth*, vol. 155, nos. 1/2, pp. 1–5, 1995.

[41] H. J. Hovel, *Solar Cells in Semiconductors and Semimetals*, vol. 11, R. K. Willardson and A. C. Beer, Eds. New York, NY, USA: Academic, 1975.

Authors' photographs and biographies not available at the time of publication.

Pursuant to the DOE Public Access Plan, this document represents the authors' peer-reviewed, accepted manuscript. The published version of the article is available from the relevant publisher.